

Regularized Halfspace Depth for Functional Data

Hyemin Yeon^{*}, Xiongtao Dai[†] and Sara Lopez-Pintado[‡]

Abstract

Data depth is a powerful nonparametric tool originally proposed to rank multivariate data from center outward. In this context, one of the most archetypical depth notions is Tukey's halfspace depth. In the last few decades notions of depth have also been proposed for functional data. However, Tukey's depth cannot be extended to handle functional data because of its degeneracy. Here, we propose a new halfspace depth for functional data which avoids degeneracy by regularization. The halfspace projection directions are constrained to have a small reproducing kernel Hilbert space norm. Desirable theoretical properties of the proposed depth, such as isometry invariance, maximality at center, monotonicity relative to a deepest point, upper semi-continuity, and consistency are established. Moreover, the regularized halfspace depth can rank functional data with varying emphasis in shape or magnitude, depending on the regularization. A new outlier detection approach is also proposed, which is capable of detecting both shape and magnitude outliers. It is applicable to trajectories in L^2 , a very general space of functions that include non-smooth trajectories. Based on extensive numerical studies, our methods are shown to perform well in terms of detecting outliers of different types. Three real data examples showcase the proposed depth notion.

Keywords and phrases: Functional data analysis; Functional rankings; Infinite dimension; Outlier detection; Robust statistics.

1 Introduction

1.1 Backgrounds and degeneracy issue

In the last several decades, data depth methods for multivariate data have been developed and are shown to be a powerful tool for both exploratory data analysis and robust statistics. Many different depth notions have been proposed, such as Tukey's halfspace depth (Tukey, 1975), simplicial depth (Liu, 1990), and Mahalanobis depth (Liu, 1992). These multivariate depth functions have not only been well-investigated theoretically (Donoho and Gasko, 1992, Zuo and Serfling, 2000) but have also been applied for handling different statistical problems (Yeh and Singh, 1997, Rousseeuw et al., 1999, Li et al., 2012).

In particular, Tukey's halfspace depth has been popular due to its many desirable properties (Zuo and Serfling, 2000) and the robustness of its depth median (Donoho and Gasko, 1992). However, its generalization to functional data inevitably encounters a degeneracy issue, namely, a naive extension of Tukey's depth has zero depth values almost surely. Intuitively, this is due to the

^{*}Department of Statistics, North Carolina State University, North Carolina 27695, U.S.A. Email: hyeon@ncsu.edu.

[†]Division of Biostatistics, University of California, Berkeley

[‡]Department of Health Sciences, Northeastern University

infinite-dimensionality of the functional space, where the set of projections is “too rich” and thus Tukey’s depth defined from the most extreme projection is too small. A numerical illustration of the degeneracy phenomenon in practice is shown in [Figure 1](#), where the naive direct extension of Tukey’s depth to functional data (red curve) assigns zero depth to the majority of observations, preventing depth comparisons. The degeneracy was first discovered by [Dutta et al. \(2011\)](#) and further investigated by [Kuelbs and Zinn \(2013\)](#), [Chakraborty and Chaudhuri \(2014a\)](#). See Table 1 of [Gijbels and Nagy \(2017\)](#) for a summary of the degeneracy issues in this and other existing functional depth notions. Tukey’s halfspace depth has therefore been practically dismissed from consideration for functional data due to the failure of the naive generalization.

1.2 Regularized halfspace depth

In this work, we propose a new notion of functional depth called the regularized halfspace depth (RHD). We resolve the degeneracy issue by restricting the set of projection directions in the definition of the halfspace depth to the set of directions with reproducing kernel Hilbert space (RKHS) norm less than a given positive number $\lambda \in (0, \infty)$. Indeed, the proposed RHD obtained in this fashion is non-degenerate over a general class of random functions. This allows for depth-based rankings if, for example, the underlying distribution of the random element is Gaussian. [Figure 1](#) illustrates that the RHD is free of the degeneracy issue as shown by the green and yellow curves for small and large λ values, while the original Tukey’s halfspace depth, corresponding to the red curve with $\lambda = \infty$, exhibits a degenerate behavior, since almost all observations have zero depth.

Details about this simulation setup can be found in ?? in the Supplemental Materials. Smaller λ results in greater regularization, in which case the distribution of the depth values become more positive and dispersed.

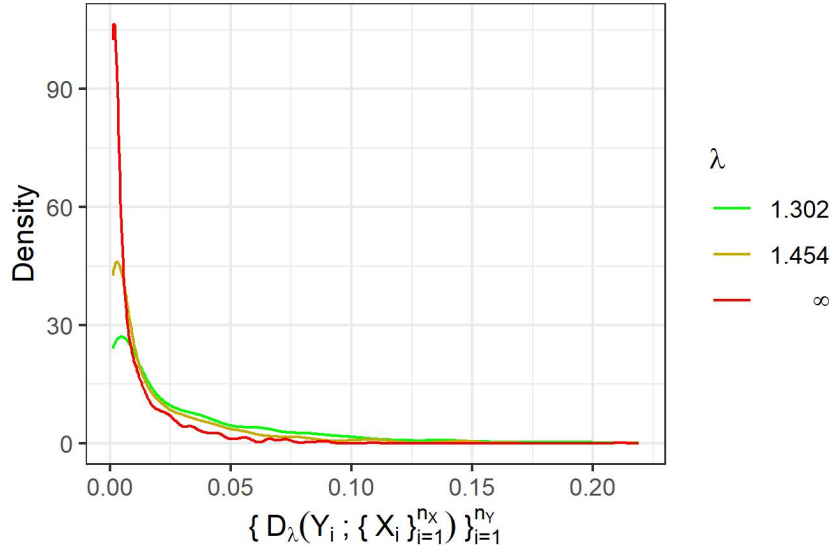


Figure 1: Distributions of the original Tukey’s halfspace depth values and the proposed regularized halfspace depth with different regularization parameters $\lambda \in \{1.302, 1.454\}$. The depth values are w.r.t. $\mathcal{X}_n \equiv \{X_i\}_{i=1}^{n_X}$ and evaluated at the points in $\mathcal{Y}_n \equiv \{Y_i\}_{i=1}^{n_Y}$, where the observations are i.i.d. realizations from a Gaussian process and $n_X = n_Y = 1000$. Tukey’s depth corresponds to $\lambda = \infty$.

A related but highly different projection-based Tukey's depth for functional data has been considered by [Cuesta-Albertos and Nieto-Reyes \(2008\)](#), who proposed the random Tukey depth which defines the depth as the most severe extremity as seen along a *fixed number* of random projections. The number of projections should not diverge to infinity because otherwise the random Tukey depth will approach Tukey's halfspace depth, which degenerates given functional observations. In contrast, our approach targets to utilize *infinitely many* projections and thus is more sensitive against different types of extremeness; the degeneracy issue is resolved through regularizing the projections. These approaches both demonstrate the necessity of applying restrictions when defining functional depth through the infimum over projection directions.

In addition to non-degeneracy, we establish other desirable depth properties for the RHD in analogy to the ones for multivariate and functional data postulated by [Zuo and Serfling \(2000\)](#), [Nieto-Reyes and Battey \(2016\)](#), and [Gijbels and Nagy \(2017\)](#), respectively. We also include topological properties of the depth level sets. A uniform consistency of the sample RHD for the population RHD is verified over a totally bounded subset. A version of the Glivenko–Cantelli theorem is derived for a class of infinite-dimensional halfspaces as a by-product. In all, our new depth satisfies all of the desirable properties considered by [Gijbels and Nagy \(2017\)](#), unlike most other existing functional depths.

A prominent feature of the RHD is its flexibility in ranking curves based on different shape features controlled by the regularization parameter λ : RHD with a larger λ emphasizes higher-frequency shape differences in the samples, while a smaller λ emphasizes overall magnitude. The definition of "shape" is data-driven and comes from the modes of variation in the observed data. This feature leads to our new definitions of extremeness for curves informed by data, which is utilized and demonstrated in other applications such as outlier detection method and will be introduced next.

1.3 Functional outlier detection

In recent years, substantial development of outlier detection methods in functional data have been accomplished by using notions of functional depth. The functional boxplot proposed by [Sun and Genton \(2011\)](#) is an extension of the original boxplot (cf. [Tukey, 1977](#)), where functional whiskers are constructed based on a functional depth method, in particular the modified band depth (MBD) ([López-Pintado and Romo, 2009](#)). Outlier detection methods for functions taking values in a multivariate space have also been considered, by e.g., [Hubert et al. \(2015\)](#).

Trajectories outlying in only shape but not at any given time point are challenging to detect; [Nagy et al. \(2017\)](#) focused on the detection of this type of outliers by applying data depths to the joint distribution of a set of two or three time points altogether. [Dai et al. \(2020\)](#) proposed to apply transformations sequentially to the functional data to reveal shape outliers that are not easily detected by other methods. Alternative outlier detection methods based on functional data depth include functional bagplots ([Hyndman and Shang, 2010](#)), the outliergram ([Arribas-Gil and Romo, 2014](#)), and directional outlyingness ([Dai and Genton, 2018](#)).

Unlike magnitude outliers that tend to have an extreme average value over the support, shape outliers are hard to define in the first place because there is vast possibility of outlyingness in shape, in terms of, e.g., jumps, peaks, smoothness, trends etc. A shape outlier can often be inlying

pointwise but has a different overall pattern than the majority of the sample curves over the support. A major benefit of the proposed RHD is that it captures different modes of variation in the sample $\mathcal{X}_n \equiv \{X_i\}_{i=1}^n$ depending on the choice of the regularization parameter λ . We propose a *data-adaptive* definition of shape outlyingness and establish a novel shape outlier detection method based on the proposed RHD. The method uses a large number of randomly drawn directions to approximate the sample RHD and applies the univariate boxplot to the data functions projected onto those directions. As provided in the numerical studies, the proposed outlier detection method well detects different types of extremeness/outlyingness in shape as well as in magnitude.

Our methods are shown to be practical and useful with different real data examples: medfly, world population growth, and sea surface temperature datasets. Due to the complexity of the first dataset, it has barely been studied (cf. [Sguera and López-Pintado, 2021](#)) in the literature of functional outlier detection, while the other two datasets have been analyzed a few times previously (cf. [Sun and Genton, 2011](#), [Nagy et al., 2017](#), [Dai et al., 2020](#)). Our data illustrations demonstrate that the proposed method is relevant for analyzing both complicated and rough trajectories as well as relatively simple smooth curves.

1.4 Contributions and outline of the paper

Next we highlight our main contributions while summarizing the organization of the paper. [Section 2](#) defines and studies the proposed RHD, which is a novel, flexible and useful depth notion for functional data; it is shown in [Section 2.1](#) that the proposed RHD is non-degenerate over a large class of random functions. We then establish desirable depth properties of the RHD in [Sections 2.2-2.3](#) and provide a theoretically reasonable and practical algorithm to compute it in [Section 2.4](#); some intermediate results such as a Glivenko-Cantelli theorem are new in the functional depth literature. The choice of relevant tuning parameters are discussed in [Section 2.5](#). [Section 3](#) is devoted to describing the proposed outlier detection method; the details are presented in [Section 3.1](#) along with a rule for selecting the adjustment factor, while [Section 3.2](#) emphasizes the robustness of the overall procedure against outliers. The proposed methods are useful and outstanding for identifying functional shape outliers, which can be challenging for the existing depth notions, as illustrated in the numerical study in [Section 4](#). Data applications are described in [Section 5](#), indicating that our methods are applicable to some complex structured functional data. All proofs, additional simulations, and extra results from the real data analyses are contained in the supplement.

2 Regularized Halfspace Depth

In [Section 2.1](#), we start by defining the regularized halfspace depth for functional data and verifying the non-degeneracy property. [Section 2.2](#) then describes and digests the desirable theoretical properties of the RHD, while [Section 2.3](#) is devoted to defining the sample version of the RHD and establishing its consistency. A practical computational algorithm for approximating the sample RHD based on random projections is provided along with its theoretical justification in [Section 2.4](#). Finally, we discuss how to select tuning parameters involved in the computation of the RHD in [Section 2.5](#).

2.1 Motivation and Definition

Let X be a random function defined on a probability space $(\Omega, \mathcal{F}, \mathbb{P})$ that takes values in the underlying Hilbert space \mathbb{H} with inner product $\langle \cdot, \cdot \rangle$. We suppose that \mathbb{H} is infinite-dimensional and separable. The original *Tukey's halfspace depth* (Tukey, 1975) of $x \in \mathbb{H}$ with respect to the probability measure P_X induced by X is, for $x \in \mathbb{H}$,

$$D(x) = D(x; P_X) = \inf_{v \in \mathbb{H}: \|v\|=1} \mathbb{P}(\langle X - x, v \rangle \geq 0). \quad (1)$$

However, since the dimension of \mathbb{H} is not finite, this naive definition is degenerate (Dutta et al., 2011) as described next.

Theorem 1 (Degeneracy of Tukey's halfspace depth). *Suppose that X is a Gaussian element. Then, it holds that $D(x; P_X) = 0$ for P_X -almost surely all $x \in \mathbb{H}$.*

We, instead, overcome this degeneracy issue and define a new notion of halfspace depth by introducing a regularization step. Let \mathbb{H} be an infinite-dimensional Hilbert space, and define by $x \otimes y : \mathbb{H} \rightarrow \mathbb{H}$, the tensor product of two elements $x, y \in \mathbb{H}$, as a bounded linear operator $(x \otimes y)(z) = \langle z, x \rangle y$ for $z \in \mathbb{H}$. Under a finite second moment assumption $\mathbb{E}[\|X\|^2] < \infty$, the covariance operator of X is defined as $\Gamma \equiv \mathbb{E}[(X - \mathbb{E}[X]) \otimes (X - \mathbb{E}[X])]$. Since the covariance operator Γ is self-adjoint, non-negative definite, and compact, by spectral decomposition, it admits the eigen-decomposition $\Gamma = \sum_{j=1}^{\infty} \gamma_j (\phi_j \otimes \phi_j)$, where (λ_j, ϕ_j) is the j -th eigenvalue–eigenfunction pair of Γ with the properties that $\gamma_1 \geq \gamma_2 \geq \dots \geq 0$, $\gamma_j \rightarrow 0$ as $j \rightarrow \infty$, and the eigenfunctions $\{\phi_j\}_{j=1}^{\infty}$ form a complete orthonormal system for the closure of the image of Γ (Hsing and Eubank, 2015). We further assume that the eigenvalues are positive and strictly decreasing, i.e., $\gamma_1 > \gamma_2 > \dots > 0$, in order to avoid the non-interesting case that X is supported only in a finite-dimensional subspace of \mathbb{H} .

The proposed regularized halfspace depth is defined next.

Definition 1. *The regularized halfspace depth (RHD) of $x \in \mathbb{H}$ with respect to P_X is defined as*

$$D_{\lambda}(x) = D_{\lambda}(x; P_X) = \inf_{v \in \mathbb{H}: \|v\|=1, \|\Gamma^{-1/2}v\| \leq \lambda} \mathbb{P}(\langle X - x, v \rangle \geq 0), \quad (2)$$

where $\lambda \in (0, \infty)$ is a regularization parameter and $\Gamma^{-1/2} \equiv \sum_{j=1}^{\infty} \gamma_j^{-1/2} (\phi_j \otimes \phi_j)$.

The set of projection directions used to define the RHD D_{λ} is written as

$$\mathcal{V}_{\lambda} \equiv \{v \in \mathbb{H} : \|v\| = 1, \|\Gamma^{-1/2}v\| \leq \lambda\}. \quad (3)$$

We refer to the norm $\|v\|_{\mathbb{H}(\Gamma)} \equiv \|\Gamma^{-1/2}v\|$ as the reproducing kernel Hilbert space (RKHS) norm because if $\mathbb{H} = L^2([0, 1])$ and X has a continuous covariance function $G(s, t) = \text{cov}(X(s), X(t))$, $s, t \in [0, 1]$, then $\mathbb{H}(\Gamma) \equiv \{v \in L^2([0, 1]) : \|\Gamma^{-1/2}v\| < \infty\}$ is an RKHS with reproducing kernel G (cf. Wahba, 1973). The definitions $\|v\|_{\mathbb{H}(\Gamma)}$ and $\mathbb{H}(\Gamma)$ are generally valid given any Hilbert space \mathbb{H} . The projections in \mathcal{V}_{λ} becomes richer as λ increases and approaches $\mathbb{H}(\Gamma)$ as $\lambda \rightarrow \infty$, where the latter is an infinite-dimensional dense subspace of \mathbb{H} .

The regularization is the key difference of our method from other existing depth notions. For $\lambda \in (0, \infty)$, we restrict the set of unit-norm projection directions used in the halfspace probabilities to \mathcal{V}_λ in (3), which requires the RKHS norm of the projections to be at most λ . This will resolve the degeneracy issue as will be shown shortly. To the best of our knowledge, regularization has never been used in the depth literature in the context of either finite or infinite dimensional spaces.

Without regularization, degeneracy occurs for original Tukey's depth in \mathbb{H} because the projection set $\mathcal{V} \equiv \{v \in \mathbb{H} : \|v\| = 1\}$ in (1) is too rich. This set contains all of the infinitely many eigenfunctions, resulting in the infimum in (1) being too small. In contrast, our projection set \mathcal{V}_λ from (3) is moderately sized, in that it contains a collection of infinite linear combinations of the eigenfunctions with the constraint that the coefficients of non-leading eigenfunctions must be small. For instance, let $a_j = [(\gamma_j 2^{-j}) / (\sum_k \gamma_k 2^{-k})]^{1/2}$ for $j = 1, 2, \dots$. If $\lambda \geq (\gamma_1/2)^{-1}$, then $\sum_j a_j \phi_j \in \mathcal{V}_\lambda$. However, $\phi_j \in \mathcal{V}_\lambda$ if and only if $\gamma_j^{-1/2} \leq \lambda$, so \mathcal{V}_λ contains only finitely many eigenfunctions; see also ?? in the supplement. This enables our proposed RHD to avoid the degeneracy as well as to become a flexible data depth method with desirable theoretical properties to be described in Section 2.2.

Theorem 2 shows that the RHD is free of degeneracy.

Theorem 2 (Non-degeneracy of the RHD). *The following holds:*

- (a) *If X is Gaussian, then we have $D_\lambda(x) > 0$ for any $x \in \mathbb{H}$.*
- (b) *Let X be a general random function and $\mu = \mathbb{E}[X]$. Suppose that (i) for some $c > 0$, we have $\mathbb{P}(\langle X - \mu, v \rangle \leq -t) \leq c\mathbb{P}(\langle X - \mu, v \rangle \geq t)$ for all $v \in \mathcal{V}_\lambda$ and $t \geq 0$; and (ii) $\mathbb{E}[\|X\|^4] < \infty$. Then $D_\lambda(x) > 0$ for any $x \in \mathbb{H}$ with $\|x - \mu\| < \lambda^{-1}$.*

The first statement shows that the regularized halfspace depth values are always positive for Gaussian functional data. The second statement shows that depth values are non-zero in a neighborhood of the mean μ , where the first condition (i) is to ensure balanced tail probabilities along the projections, and the moment condition in (ii) is to guarantee non-negligible tail probabilities. The class of random functions satisfying these conditions (i)-(ii) in Theorem 2(b) includes many well-known distributions such as t - and χ^2 -distributions.

In addition to resolving degeneracy, regularization λ also provides flexibility on emphasizing the shape and/or magnitude of the functional observations. Given a small λ , the RHD focuses more on the overall magnitude of the input functions because the projection set concentrates around the leading eigenfunctions, which tend to capture lower frequency variations. On the other hand, as λ increases, the RHD increases its emphasis on variation along the higher-frequency directions given by the non-leading eigenfunctions. This property of the RHD will be utilized later for shape outlier detection.

Our proposed RHD can be constructed whenever the underlying function space is a separable Hilbert space, for example, $L^2 \equiv L^2([0, 1]) = \left\{ f : [0, 1] \rightarrow \mathbb{R} \mid \int_0^1 f(t)^2 dt < \infty \right\}$ with inner product $\langle f_1, f_2 \rangle \equiv \int_0^1 f_1(t)f_2(t)dt$ for $f_1, f_2 \in L^2$. More generally, the RHD is also applicable to functional data taking values in a multivariate space (cf. [Claeskens et al., 2014](#), [Hubert et al., 2015](#), [López-Pintado et al., 2014](#)) given an appropriately defined inner product. For solidity, in this work, we focus on univariate curves in $\mathbb{H} = L^2$.

2.2 Theoretical Properties

For a depth function to be intuitively sound, it should provide a center-outward ordering of the data and satisfy some desirable properties. [Liu \(1990\)](#) discussed some properties satisfied by the proposed simplicial depth. [Zuo and Serfling \(2000\)](#) formally postulated a list of desirable properties that should be satisfied by a well-designed depth function and showed that the original Tukey's halfspace depth satisfies all these properties. [Nieto-Reyes and Battey \(2016\)](#), [Gijbels and Nagy \(2017\)](#) among others extended such depth properties for functional data. We show some basic properties of the RHD in the following theorems after extending the postulation of the depth properties by [Zuo and Serfling \(2000\)](#) to the infinite-dimensional Hilbert space \mathbb{H} . The proofs are deferred to ?? in the Supplementary Materials.

Theorem 3.

- (a) (*Isometry invariance*) Let $A : \mathbb{H} \rightarrow \mathbb{H}$ is a bounded linear operator and $b \in \mathbb{H}$. If A is a surjective isometry, then we have $D_\lambda(Ax + b, P_{AX+b}) = D_\lambda(x, P_X)$ for each $x \in \mathbb{H}$.
- (b) (*Maximality at center*) Suppose that X is halfspace symmetric about a unique center $\mu \in \mathbb{H}$ in the sense that $P_X(H) \geq 1/2$ for each $H \in \mathcal{H}(\mu)$, where $\mathcal{H}(x)$ denotes the collection of all closed halfspaces containing $x \in \mathbb{H}$. Then, if $\lambda > \gamma_1^{-1/2}$ where γ_1 is the largest eigenvalue, we have $D_\lambda(\mu) = \sup_{x \in \mathbb{H}} D_\lambda(x)$.
- (c) (*Monotonicity relative to deepest point*) Let $\theta \in \mathbb{H}$ be such that $D_\lambda(\theta) = \sup_{x \in \mathbb{H}} D_\lambda(x)$. Then, it holds for any $x \in \mathbb{H}$ that $D_\lambda(x) \leq D_\lambda(\theta + \alpha(x - \theta))$, $\alpha \in [0, 1]$.
- (d) (*Vanishing at infinity*) Let $\mathbb{V} \equiv \text{span}\{\phi_1, \dots, \phi_m\} \subseteq \mathbb{H}$ be the subspace spanned by the first m eigenfunctions. Then, for any sequence $\{x_n\} \subseteq \mathbb{V}$ with $\|x_n\| \rightarrow \infty$ as $n \rightarrow \infty$, we have $D_\lambda(x_n) \rightarrow 0$ as $n \rightarrow \infty$.

[Theorem 3\(a\)](#) extends the affine invariance property (cf. [Zuo and Serfling, 2000](#)) to an infinite dimensional space and establishes this property for the proposed RHD because any surjective isometry between two normed spaces is affine by the Mazui–Ulam theorem ([Väisälä, 2003](#)). Properties (b) and (c) in [Theorem 3](#) respectively states that the RHD is maximized at the unique center μ and it is nonincreasing along any ray leaving from the deepest curve $\mu \in \mathbb{H}$. These properties are analogous of their Euclidean versions in [Zuo and Serfling \(2000\)](#), but the proof for (b) is more involved and uses properties of the projection set \mathcal{V}_λ . [Theorem 3\(d\)](#) is a weakened version of vanishing at infinity property where we need the finite-dimensional subspace assumption to limit the behavior of the depth function; see ?? in the Supplementary Materials for a counterexample.

The next theorem establishes the continuity of the depth function and topological properties of its level sets. For $\tau \in [0, \infty)$, we define the *upper level set* $G_{\tau, \lambda}$ of D_λ at level τ as $G_{\tau, \lambda} \equiv \{x \in \mathbb{H} : D_\lambda(x) \geq \tau\}$. The following theorem extends analogous properties for finite-dimensional data shown in Theorem 2.11 of [Zuo and Serfling \(2000\)](#).

Theorem 4.

- (a) The depth function $D_\lambda : \mathbb{H} \rightarrow [0, \infty)$ is upper semi-continuous.

- (b) The upper level sets $\mathcal{G}_\lambda \equiv \{G_{\tau,\lambda}\}_{\tau \in [0,\infty)}$ are nested, closed (hence, complete), and convex in \mathbb{H} .
- (c) Let $\mathbb{V} \equiv \text{span}\{\phi_1, \dots, \phi_m\} \subseteq \mathbb{H}$ be a finite-dimensional subspace spanned by the first m eigenfunctions. Then, for any τ , $G_{\tau,\lambda} \cap \mathbb{V}$ is compact.

The upper semi-continuity of the RHD D_λ and the closedness (and hence, the completeness) of the level set $G_{\tau,\lambda}$ are closely related. The compactness follows from vanishing at infinity and the restriction onto a finite dimensional subspace of \mathbb{H} . Without this restriction, the compactness of the level sets may not be achieved as described in ?? of the Supplementary Materials since vanishing at infinity fails.

2.3 Sample RHD and its Consistency

The population version of the RHD from (2) cannot be computed in practice. To define its sample version estimated from the observed functions, let X_1, \dots, X_n be independent and identically distributed (iid) copies of X with empirical distribution \hat{P}_n defined as $\hat{P}_n(B) \equiv n^{-1} \sum_{i=1}^n \mathbb{I}(X_i \in B)$ for a Borel set $B \in \mathcal{B}(\mathbb{H})$, where \mathbb{I} denotes the indicator function.. The sample covariance operator $\hat{\Gamma}_n$ is defined as $\hat{\Gamma}_n \equiv n^{-1} \sum_{i=1}^n (X_i - \bar{X}) \otimes (X_i - \bar{X})$ with sample mean $\bar{X} \equiv n^{-1} \sum_{i=1}^n X_i$. Write the spectral decomposition of the operator $\hat{\Gamma}_n$ as $\hat{\Gamma}_n = \sum_{j=1}^n \hat{\gamma}_j (\hat{\phi}_j \otimes \hat{\phi}_j)$, where $(\hat{\lambda}_j, \hat{\phi}_j)$ is the j -th eigenpair of $\hat{\Gamma}_n$ for $j = 1, \dots, n$, with $\hat{\gamma}_1 \geq \dots \geq \hat{\gamma}_n \geq 0$ (Hsing and Eubank, 2015).

To define the sample version of the RHD, the set of projection directions is obtained as

$$\hat{\mathcal{V}}_{\lambda,J} \equiv \{v \in \text{span}\{\hat{\phi}_1, \dots, \hat{\phi}_J\} : \|v\| = 1, \|\hat{\Gamma}_J^{-1/2} v\| \leq \lambda\},$$

where $\hat{\Gamma}_J^{-1/2} \equiv \sum_{j=1}^J \hat{\gamma}_j^{-1/2} \hat{\phi}_j$ is a J -truncated inverse of the square root operator $\hat{\Gamma}_n^{1/2} = \sum_{j=1}^n \hat{\gamma}_j^{1/2} \hat{\phi}_j$. Here, the truncation parameter $J = J(n)$ may depend on the sample size n with $J(n) \rightarrow \infty$ as $n \rightarrow \infty$. We define the *sample RHD* of $x \in \mathbb{H}$ (with respect to \hat{P}_n) as

$$\hat{D}_{\lambda,n}(x) = \hat{D}_{\lambda,n}(x, \hat{P}_n) = \inf_{v \in \hat{\mathcal{V}}_{\lambda,J}} n^{-1} \sum_{i=1}^n \mathbb{I}(\langle X_i - x, v \rangle \geq 0). \quad (4)$$

To establish the uniform consistency of the sample RHD $\hat{D}_{\lambda,n}(x)$ for the population RHD $D_\lambda(x)$, we need the following continuity/anti-concentration assumption imposed on the distribution of the projection of X : for a regularization parameter $\lambda \in (0, \infty)$ and a totally bounded subset $\mathbb{B} \subseteq \mathbb{H}$,

$$\text{Condition } C(\lambda, \mathbb{B}): \lim_{r \rightarrow 0} \limsup_{k \rightarrow \infty} \sup_{x \in \mathbb{B}, v \in \mathcal{V}_\lambda} \mathbb{P}(|\langle X - x, \Pi_k v \rangle| \leq r) = 0,$$

where $\Pi_k \equiv \sum_{l=1}^k (\phi_k \otimes \phi_k)$ denotes the projection operator onto the linear space spanned by the first k eigenfunctions for integer $k \geq 1$.

This condition is satisfied by a large class of random functions X where the projection scores $\langle X, \phi_j \rangle$, $j = 1, 2, \dots$ are independent and continuous; in particular, Gaussian random functions.

Example 1. If X is Gaussian, for each $v \in \mathcal{V}_\lambda$ and $x \in \mathbb{B}$, a truncated projection $\langle X - x, \Pi_k v \rangle$ follows the normal distribution with mean $\langle \mu - x, \Pi_k v \rangle$ and variance $\|\Gamma^{1/2} \Pi_k v\|^2$. Here, $\Pi_k v \neq 0$

for all \mathcal{V}_λ and for sufficiently large k by ?? in the supplement. Moreover, the mean and standard deviation are bounded by ?? as $\sup_{x \in \mathbb{B}, v \in \mathcal{V}_\lambda} |\langle \mu - x, \Pi_k v \rangle| \leq \|\mu\| + \sup_{x \in \mathbb{B}} \|x\| < \infty$ and $\liminf_{k \rightarrow \infty} \inf_{v \in \mathcal{V}_\lambda} \|\Gamma^{1/2} \Pi_k v\| \geq (2\lambda)^{-1} > 0$. By the properties of normal distribution,

$$\limsup_{k \rightarrow \infty} \sup_{x \in \mathbb{B}, v \in \mathcal{V}_\lambda} \mathbb{P}(|\langle X - x, \Pi_k v \rangle| \leq \tau) \leq \Phi(2\lambda\tau) - \Phi(-2\lambda\tau) \rightarrow 0$$

as $\tau \rightarrow 0$. Hence, Condition $C(\lambda, \mathbb{B})$ holds for Gaussian element X .

To verify the consistency theorem, in addition to Condition $C(\lambda, \mathbb{B})$, we impose some standard regularity conditions on X , denoted as Conditions (A1)-(A4) in ?? of the supplement. Similar or stronger conditions are commonly imposed in the functional principal component analysis literature for consistent estimation of the eigen-components (Cardot et al., 2007, Hall et al., 2007). These conditions are applied in the proofs involving perturbation theory for functional data (cf. Sections ??-?? of the supplement). The consistency result is established in the following theorem.

Theorem 5. *Let $\lambda \in (0, \infty)$ and $\mathbb{B} \subseteq \mathbb{H}$ be a totally bounded subset. Suppose that Condition $C(\lambda + \lambda_0, \mathbb{B})$ holds for some $\lambda_0 \in (0, \infty)$, Conditions ??-?? in the supplement hold, and $n^{-1/2} J^{7/2} (\log J)^2 = O(1)$ as $n \rightarrow \infty$. Then, as $n \rightarrow \infty$, we have*

$$\sup_{x \in \mathbb{B}} |\hat{D}_{\lambda, n}(x) - D_\lambda(x)| \xrightarrow{\mathbb{P}} 0.$$

The proof for this result is included in the Appendix. A main component of the proof is to establish the Glivenko–Cantelli theorem for the empirical process $\{\hat{P}_n(H_{x, v}) : v \in \mathcal{V}_\lambda, x \in \mathbb{B}\}$ indexed by an infinite-dimensional class of halfspaces, where $H_{x, v} \equiv \{y \in \mathbb{H} : \langle y - x, v \rangle \geq 0\}$ denote the closed halfspace with normal vector $v \in \mathbb{H}$ containing $x \in \mathbb{H}$ on its boundary. Empirical process results for functional depth are challenging to show and have rarely been studied, except for Glivenko–Cantelli and Donsker theorems for spatial depth by Chakraborty and Chaudhuri (2014b) where the index set is restricted to some finite dimensional subspace. Here, we consider a projection set \mathcal{V}_λ containing infinite-dimensional projections, which is more involved. The proof consists of showing the total boundedness of \mathcal{V}_λ and asymptotic uniform equicontinuity of the stochastic process $\{\hat{P}_n(H_{x, v}) : v \in \mathcal{V}_\lambda, x \in \mathbb{B}\}$ (cf. ?? of the supplement).

2.4 Practical Computation

The sample RHD involves an infimum over the projection set $\hat{\mathcal{V}}_{\lambda, J}$ which makes the computation hard; even for the original Tukey's depth in \mathbb{R}^d the exact computation can be prohibitive for dimension $d \geq 4$ (Dyckerhoff and Mozharovskyi, 2016). To approximate the sample RHD, we adopt a random projection approach.

For $\hat{v} = \sum_{j=1}^J \hat{a}_j \hat{\phi}_j \in \text{span}\{\hat{\phi}_1, \dots, \hat{\phi}_J\}$ with $\hat{\mathbf{a}} = (\hat{a}_1, \dots, \hat{a}_J)^\top \in \mathbb{R}^J$, it holds that

$$\|\hat{v}\|^2 = \sum_{j=1}^J \hat{a}_j^2 = \|\hat{\mathbf{a}}\|_{\mathbb{R}^J}^2 \quad \text{and} \quad \|\hat{\Gamma}_J^{-1/2} \hat{v}\|^2 = \sum_{j=1}^J \hat{\gamma}_j^{-1} \hat{a}_j^2 = \|\hat{\mathcal{R}}_J^{-1/2} \hat{\mathbf{a}}\|_{\mathbb{R}^J}^2$$

where $\hat{\mathcal{R}}_J \equiv \text{diag}(\hat{\gamma}_1, \dots, \hat{\gamma}_J)$. Then, $\hat{\mathcal{V}}_{\lambda,J}$ can be written as

$$\hat{\mathcal{V}}_{\lambda,J} = \left\{ \hat{v} = \sum_{j=1}^J \hat{a}_j \hat{\phi}_j \in \text{span}\{\hat{\phi}_1, \dots, \hat{\phi}_J\} : \hat{\mathbf{a}} = (\hat{a}_1, \dots, \hat{a}_J)^\top \in \hat{\mathcal{A}}_{\lambda,J} \right\}$$

where $\hat{\mathcal{A}}_{\lambda,J} \equiv \{\hat{\mathbf{a}} \in \mathbb{R}^J : \|\hat{\mathbf{a}}\|_{\mathbb{R}^J} = 1, \|\hat{\mathcal{R}}_J^{-1/2} \hat{\mathbf{a}}\|_{\mathbb{R}^J} \leq \lambda\}$. Note that the set $\hat{\mathcal{A}}_{\lambda,J}$ is the intersection of the (surface of) unit sphere and a (solid) ellipsoidal region centered at the origin in \mathbb{R}^J . Then, the sample RHD is written as

$$\hat{D}_{\lambda,n}(x) = \inf_{\hat{\mathbf{a}} \in \hat{\mathcal{A}}_{\lambda,J}} n^{-1} \sum_{i=1}^n \mathbb{I}((\hat{\mathbf{X}}_i - \hat{\mathbf{x}})^\top \hat{\mathbf{a}} \geq 0) \quad (5)$$

where $\hat{\mathbf{X}}_i = [\langle X_i, \hat{\phi}_j \rangle]_{1 \leq j \leq J}$ and $\hat{\mathbf{x}} = [\langle x, \hat{\phi}_j \rangle]_{1 \leq j \leq J}$ are J -dimensional vectors in \mathbb{R}^J . Although (5) is reminiscent of sample Tukey's depth applied on the data $\hat{\mathbf{X}}_i$, they are remarkably different in their designs. The RHD targets infinite-dimensional data and allows for an increasing J . The depth values are insensitive to increase in J when it is moderately large ($J \geq 6$ as demonstrated in our numerical studies) thanks to the regularization set which stabilizes the depth. On the other hand, Tukey's depth is most often applied in a fixed low dimension; when the dimension increases, Tukey's depth become less capable of distinguishing points because of the concentration of measure and the degeneracy issue.

To approximate the infimum, we draw M random vectors $\hat{\mathbf{a}}_m = (\hat{a}_{m1}, \dots, \hat{a}_{mJ})^\top \stackrel{\text{iid}}{\sim} \nu$ for $m = 1, \dots, M$ from some continuous distribution ν supported on $\hat{\mathcal{A}}_{\lambda,J} \subseteq \mathbb{R}^J$. The projection set is approximated by the finite set

$$\tilde{\mathcal{V}}_{\lambda,J,M} \equiv \left\{ \tilde{v} = \sum_{j=1}^J \hat{a}_{mj} \hat{\phi}_j : m = 1, \dots, M \right\}. \quad (6)$$

Then, the sample depth $\hat{D}_{\lambda,n}(x) = \hat{D}_{\lambda,n}(x, \hat{P}_n)$ in (5) is approximated by

$$\tilde{D}_{\lambda,n,M}(x) = \tilde{D}_{\lambda,n,M}(x, \hat{P}_n, \{\hat{\mathbf{a}}_m\}_{m=1}^M) = \min_{m=1, \dots, M} n^{-1} \sum_{i=1}^n \mathbb{I}((\hat{\mathbf{X}}_i - \hat{\mathbf{x}})^\top \hat{\mathbf{a}}_m \geq 0). \quad (7)$$

Rejection sampling is applied to draw the projection directions $\hat{\mathbf{a}}_m$. To increase acceptance in the target region $\hat{\mathcal{A}}_{\lambda,J}$, we set the proposal distribution of projection directions $\hat{\mathbf{a}}_m$ to that of $\mathbf{z}/\|\mathbf{z}\|_{\mathbb{R}^J}$ where $\mathbf{z} \sim \mathbf{N}(\mathbf{0}, \hat{\mathcal{R}}_J)$, a non-isotropic distribution on the unit sphere.

The following theorem justifies the approximated sample RHD in (7) for a sufficiently large M , for which the proof is given in ?? in the supplement.

Theorem 6. *Let $\lambda \in (0, \infty)$ and $\mathbb{B} \subseteq \mathbb{H}$ be a totally bounded subset. Suppose that the assumptions in Theorem 5 hold. Then, for each $\varepsilon > 0$, the following event occurs with probability tending to 1 as $n \rightarrow \infty$: for a continuous probability distribution ν supported on $\hat{\mathcal{A}}_{\lambda,J}$ and a sequence $\{\hat{\mathbf{a}}_m\}_{m=1}^\infty$ of iid random vectors drawn from ν , as $M \rightarrow \infty$,*

$$\nu \left(\sup_{x \in \mathbb{B}} \left| \tilde{D}_{\lambda,n,M}(x) - \hat{D}_{\lambda,n}(x) \right| > \varepsilon \right) \rightarrow 0.$$

The key point of the proof is to show a type of asymptotic equicontinuity of a process $\{\hat{P}_n(H_{x,\hat{v}}) : x \in \mathbb{B}, \hat{v} \in \hat{\mathcal{V}}_{\lambda,J}\}$, where the index set also depends on the observed random functions $\mathcal{X}_n \equiv \{X_i\}_{i=1}^n$. Such processes with a changing index set following the sample size n have rarely been studied. We derived this theorem by constructing a correspondence from $\hat{\mathcal{V}}_{\lambda,J}$ to \mathcal{V}_λ , relating this correspondence with the asymptotic equicontinuity of the original process $\{\hat{P}_n(H_{x,v}) : x \in \mathbb{B}, v \in \mathcal{V}_\lambda\}$, and using the total boundedness of \mathcal{V}_λ .

The population (2) and sample RHD (4) are monotonically decreasing as λ increases. In order for the approximate RHD to enjoy the same property, namely $\lambda \mapsto \tilde{D}_{\lambda,n,M}(x)$ is decreasing in λ when all other quantities are fixed, we employ the following procedure. Let $\Lambda \equiv \{\lambda_1, \dots, \lambda_Q\}$ be a finite set of regularization parameters that we will use to evaluate the approximate RHD. We draw a single set of random directions $\mathbf{z}_1, \dots, \mathbf{z}_M \sim \mathcal{N}(0, \hat{\mathcal{R}}_J)$ and set $\hat{\mathbf{a}}_m = \mathbf{z}_m / \|\mathbf{z}_m\|_{\mathbb{R}^J}$ as explained above, and use the directions $\{\hat{\mathbf{a}}_m\}_{m=1}^M$ to compute all depth values $\{\tilde{D}_{\lambda,n,M} : \lambda \in \Lambda\}$. The monotonicity then follows from the definition of $\tilde{D}_{\lambda,n,M}$.

In practice, instead of specifying λ for regularization, we use the u -quantile of the RKHS norms $\mathcal{N}_M \equiv \{\|\hat{\mathcal{R}}_J^{-1/2} \hat{\mathbf{a}}_m\|_{\mathbb{R}^J}\}_{m=1}^M$ as λ , where $u \in (0, 1)$ is called the *quantile level* for regularization. The quantile level approach to determine λ has several advantages; it depends on the data and avoids choosing values of λ outside of the range of the RKHS norms \mathcal{N}_M . In our numerical studies, we investigate the performance of RHD using different u -quantiles of \mathcal{N}_M as regularization parameter λ .

[Algorithm 1](#) summarizes the approximate computation.

Algorithm 1: Approximate sample RHD

Data: Random sample \mathcal{X} and depth evaluation point x
Parameters: Either regularization parameter set Λ or quantile level set \mathcal{U} . Also truncation parameter J
Result: Approximate sample RHD $\tilde{D}_{\lambda,n,M}(x)$ for $\lambda \in \Lambda$

```

1 for  $m = 1, \dots, M$  do
2   | Generate  $\mathbf{z}_m \sim \mathcal{N}(0, \hat{\mathcal{R}}_J)$  and compute  $\hat{\mathbf{a}}_m = \mathbf{z}_m / \|\mathbf{z}_m\|_{\mathbb{R}^J}$ 
3 end
4 if  $\Lambda$  is unspecified then
5   | for  $u \in \mathcal{U}$  do
6     |   Add the  $u$ -quantile of  $\{\|\hat{\mathcal{R}}_J^{-1/2} \hat{\mathbf{a}}_m\|_{\mathbb{R}^J}\}_{m=1}^M$  to  $\Lambda$ 
7   | end
8 end
9 for  $\lambda \in \Lambda$  do
10  |  $\tilde{\mathcal{A}}_{\lambda,J,M} \leftarrow \emptyset$ 
11  | for  $m = 1, \dots, M$  do
12  |   | if  $\|\hat{\mathcal{R}}_J^{-1/2} \hat{\mathbf{a}}_m\|_{\mathbb{R}^J} \leq \lambda$  then
13  |   |   | Add  $\hat{\mathbf{a}}_m$  to  $\tilde{\mathcal{A}}_{\lambda,J,M}$ 
14  |   | end
15  | end
16  |  $\tilde{D}_{\lambda,n,M}(x) \leftarrow \min_{\hat{\mathbf{a}} \in \tilde{\mathcal{A}}_{\lambda,J,M}} n^{-1} \sum_{i=1}^n \mathbb{I}((\hat{\mathbf{X}}_i - \hat{\mathbf{x}})^\top \hat{\mathbf{a}} \geq 0);$ 
17 end

```

2.5 Selecting Tuning Parameters

The approximate sample RHD $\tilde{D}_{\lambda,n,M}$ (7) involves three tuning parameters: the regularization parameter λ (or equivalently, the quantile level u), the truncation level J , and the number M of random projection directions. The most important parameter, by far, is λ since it determines how sensitive the depth is to different modes of variation in the sample, which is a useful feature for analysis. When λ is small, projections are constrained to have large components only along the leading eigenfunctions, in which case the RHD emphasizes the overall magnitude rather than shape of the curves. In contrast, when λ is large, the RHD considers projections along both leading and later eigenfunctions, so it increases its emphasis in shape relative to magnitude. This flexibility of the RHD is used and highlighted in our outlier detection method proposed in [Section 3](#) and is demonstrated numerically in [Section 4.3](#).

The choice of λ may depend on the structure of a given dataset and the purpose of the study. If a dataset can be explained by a few modes of variation (say, mostly in terms of a vertical shift), a small regularization parameter can be chosen; otherwise a larger regularization parameter should be considered. If a class label response exists, the selection of λ can be tied to depth-based classification performance ([Ghosh and Chaudhuri, 2005](#), [López-Pintado and Romo, 2006](#), [Hubert et al., 2017](#)). Parameter λ could also be chosen by maximizing the power of RHD-based rank test (for general depth-based rank test, see [Liu and Singh, 1993](#), [López-Pintado and Romo, 2009](#)) if training samples are available. In general, practitioners could inspect a range of λ values and obtain different rankings and outlyingness from the depth values. This would help understand the dataset from different perspectives in terms of magnitude vs shape. For practical uses, we recommend as default to set λ according to a quantile level $u = 0.95$ of the RKHS norms \mathcal{N}_M , which is implemented in our R package. This choice tends to display extremeness in both magnitude and shape while avoiding degeneracy as shown in our numerical studies.

The selection of the truncation level J is a secondary consideration. It should be chosen as a large enough value because J is needed for approximating the population RKHS norm $\|\Gamma^{-1/2}v\|$

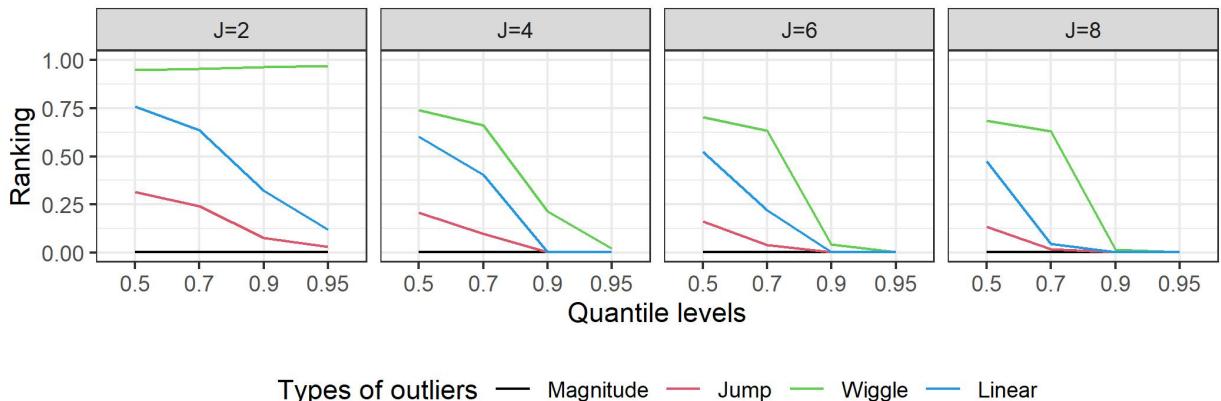


Figure 2: RHD-based normalized rankings of outlying curves selected among the ones described in [Section 4.1](#) when $n = 400$. The least deep curves have 0 normalized rank. The results show different truncation levels $J \in \{2, 4, 6, 8\}$ (panels) and four regularization parameters corresponding to the quantile levels $u \in \{0.5, 0.7, 0.9, 0.95\}$ (x-axis).

by the sample version $\|\hat{\Gamma}_J^{-1/2}v\|$. In [Figure 2](#), we show the rankings of several types of outliers when using the approximate RHD based on different λ and J parameters to illustrate how sensitive the rankings are to the choice of these parameters. A simulated dataset containing non-Gaussian functional data is considered where one outlier is added at a time.

A magnitude and three shape outliers of different types were ranked, where the x -axis and different panels display varying λ and J , respectively (see [Section 4.1](#) for more details). We define the RHD-based (normalized) rank of a functional observation X_i in the sample $\{X_i\}_{i=1}^n$ as \tilde{R}_i/n , where \tilde{R}_i denotes the rank of $\tilde{D}_{\lambda,n,M}(X_i)$ in $\{\tilde{D}_{\lambda,n,M}(X_i)\}_{i=1}^n$, and therefore, higher ranks correspond to larger depth. Minimum ranks are assigned to curves with the same depths. We observe that the results are highly similar when J is moderately large, for example, $J \geq 6$ in this case. In contrast, the rankings for the smallest and largest regularization λ are markedly different; the magnitude outlier gets the lowest rank for all λ s but this is not the case for the shape outliers. The shape outliers are only detected with higher λ s because larger λ emphasizes shape more strongly.

The least consequential parameter is M , which should be chosen to be as large as computation affords. In practice, for example, $M = 1000$ is often enough to get a reasonable approximation.

In sum, we recommend to choose a large M , a sufficiently large J that may depend on the sample size n , and an appropriate λ for the purposes of the analysis.

3 Outlier Detection

In this section, we describe an outlier detection method developed from the proposed RHD, which detects shape as well as magnitude outliers. Since having a low depth value is not sufficient to be considered an outlier, we introduce a novel outlier detection method based on projection directions in [\(6\)](#). The overall idea is to first prescreen potential outliers using the RHD, and then detect outliers by applying univariate boxplots to data projected onto restricted directions that maximally separate inliers and outliers. Comprehensive numerical studies in [Section 4.3](#) and the supplement show that our new outlier detection method works well and detects outliers with different complicated shapes.

3.1 Outlier detection procedure based on the RHD

The detailed outlier detection procedure is described as follows. We start by defining the most extreme functions with the least (approximate) RHD values as outlier candidates, for which the index set is denoted as

$$\mathcal{I}_{\min,\lambda} = \mathcal{I}_{\min,\lambda}(\mathcal{X}_n) \equiv \operatorname{argmin}_{1 \leq i \leq n} \tilde{D}_{\lambda,n,M}(X_i).$$

Let X_{i_0} , $i_0 \in \mathcal{I}_{\min,\lambda}$ be an outlier candidate in the sample $\mathcal{X}_n \equiv \{X_i\}_{i=1}^n$. To construct univariate boxplots, we keep track of only the most extreme projection directions for evaluating the halfspace probabilities at $x = X_{i_0}$ for outlier detection. Among directions in $\tilde{\mathcal{V}}_{\lambda,J,M}$ [\(6\)](#), suppose that there are $K = K_{i_0}$ directions, denoted as $\{v_{m_k}\}_{k=1}^K$, that minimize the halfspace probability when computing $\tilde{D}_{\lambda,n,M}(X_{i_0})$ in [\(7\)](#), that is,

$$\{v_{m_k}\}_{k=1}^K \subset \operatorname{argmin}_{1 \leq m \leq M} \hat{P}_n(H_{X_{i_0}, v_m}).$$

For each direction v_{m_k} , we obtain projections $\{\langle X_i, v_{m_k} \rangle\}_{i=1}^n$ and label outliers using a univariate boxplot with a given factor f to construct the fence. The fence is constructed as $[Q_1 - f \times IQR, Q_3 + f \times IQR]$ where Q_1 , Q_3 , and IQR denoting the first quartile, third quartile, and the interquartile range of the projections, respectively. We label as outliers $\mathcal{O}_{i_0, k}$ the functional observations with projection lying outside of the fence along this direction. The final set of all outliers is obtained as

$$\mathcal{O}_\lambda \equiv \left(\bigcup_{i_0 \in \mathcal{I}_{\min, \lambda}} \bigcup_{k=1}^{K_{i_0}} \mathcal{O}_{i_0, k} \right) \cap \mathcal{I}_{\min, \lambda}.$$

The algorithm for outlier detection is given in [Algorithm 2](#).

Algorithm 2: Detect outliers in \mathcal{X}_n based on the RHD

Data: Random sample \mathcal{X}_n
Parameters: Regularization λ , truncation J , and adjustment factor f
Result: Indices \mathcal{O}_λ of outliers in \mathcal{X}_n

- 1 Obtain $\tilde{D}_{\lambda, n, M}(x), x \in \mathcal{X}_n$ by invoking [Algorithm 1](#)
- 2 $\mathcal{I}_{\min, \lambda} \leftarrow \operatorname{argmin}_{1 \leq i \leq n} \tilde{D}_{\lambda, n, M}(X_i)$
- 3 $\mathcal{O}_\lambda \leftarrow \emptyset$
- 4 **for** $i_0 \in \mathcal{I}_{\min, \lambda}$ and $\hat{\mathbf{a}} \in \tilde{\mathcal{A}}_{\lambda, J}$ **do**
- 5 $x \leftarrow X_{i_0}$, $\hat{\mathbf{X}}_i \leftarrow [\langle X_i, \hat{\phi}_j \rangle]_{1 \leq j \leq J}$, and $\hat{\mathbf{x}} \leftarrow [\langle x, \hat{\phi}_j \rangle]_{j=1}^J$
- 6 **if** $n^{-1} \sum_{i=1}^n \mathbb{I}((\hat{\mathbf{X}}_i - \hat{\mathbf{x}})^\top \hat{\mathbf{a}} \geq 0) = \tilde{D}_{\lambda, n, M}(x)$ **then**
- 7 Form projections $\{\langle \hat{\mathbf{X}}_i, \hat{\mathbf{a}} \rangle\}_{i=1}^n$ and obtain their first quartile, third quartile, and interquartile range as Q_1 , Q_3 , and IQR
- 8 **for** $i = 1, \dots, n$ **do**
- 9 **if** $\langle \hat{\mathbf{X}}_i, \hat{\mathbf{a}} \rangle \notin [Q_1 - f \cdot IQR, Q_3 + f \cdot IQR]$ **then**
- 10 $\mathcal{O}_\lambda \leftarrow \mathcal{O}_\lambda \cup \{i\}$
- 11 **end**
- 12 **end**
- 13 **end**
- 14 **end**
- 15 $\mathcal{O}_\lambda \leftarrow \mathcal{O}_\lambda \cap \mathcal{I}_{\min, \lambda};$

We determine the adjustment factor f in our outlier detection method by a simulation-based method, following the approach in [Sun and Genton \(2012\)](#). The factor f in the functional boxplot is calibrated to the value that assigns 0.7% observations as outliers in simulated datasets containing only inliers. The simulated observations follow a Gaussian distribution matching the (empirical) mean and covariance functions of the actual input dataset. See ?? in the supplement.

Remark 1. *In our paper, we only considered functional observations without clusters. Such cases can be reduced to solving classification or clustering problems, which might require different tools such as DD-plot ([Li et al., 2012](#)) or local depth ([Paindaveine and Van Bever, 2013](#)). However, these problems are beyond the scope of our paper, and we leave them as future directions.*

3.2 Robustness of the RHD

With a broader interpretation of robustness, the proposed RHD is robust in the following sense. First, outliers, even very extreme ones, will not break down our RHD-based outlier detection method as shown in our simulation study (cf. [Section 4](#)). This might sound surprising because our

procedure relies on the covariance operator Γ which is non-robust, but the sensitivity to outliers actually helps reveal shape outliers by capturing the directions where these outliers lie. Second, the choice of the adjustment factor f by ?? in the supplement is shown to be resistant to outliers, as discussed in Section S4 of the supplement, even though the procedure depends on the sample covariance operator $\hat{\Gamma}_n$ which is (again) non-robust. This indicates that the whole procedure of our outlier detection method is robust even against very extreme outliers and useful for detecting all types of outliers under our consideration.

4 Numerical Studies

Section 4.1 describes the design of the simulation study along with different types of magnitude and shape outliers under consideration. The performances of the RHD and the proposed outlier detection method are respectively evaluated in Section 4.2 and Section 4.3.

The performance of the RHD is evaluated based on (i) the depth ranks of the outliers in Section 4.2, and (ii) the proportions of falsely/correctly detected outliers in Section 4.3. For the first study, we compared RHD with other depth notions including MBD (López-Pintado and Romo, 2009), extremal depth (ED) (Narisetty and Nair, 2016), as well as the k -th order integrated depth by Nagy et al. (2017), denoted as Nagy_k with order $k \in \{1, 2, 3\}$. In the second study, we compared our proposed outlier detection method against functional boxplot (Sun and Genton, 2011) constructed based on either the MBD or the ED, and with the method introduced in Nagy et al. (2017). All these methods are implemented in R packages `fdaoutlier` and `ddalpha`. Since all outlier detection methods are able to benefit from transformations, e.g., computing derivatives of the original curve, (cf. Nagy et al., 2017, Section 3.1; Dai et al. (2020)), we consider only detection methods based on the original curves for simplicity.

4.1 Setting up different types of outliers

To evaluate the performance of our proposed RHD, we consider inliers that are relatively smooth curves and different types of outliers, which include outliers in either magnitude or shape. The shape outliers are outlying only in terms of their pattern but not in magnitude. All curves are evaluated at 50 equally spaced time points in $[0, 1]$.

Inlier curves $\mathcal{X}_{n_{in}} = \{X_i\}_{i=1}^{n_{in}}$ are generated as

$$X = \sum_{j=1}^{J_0} \sqrt{\gamma_j} \xi_j \phi_j \quad (8)$$

with $J_0 = 15$, where $\{\gamma_j\}_{j=1}^{\infty}$ is a non-increasing sequence of positive numbers with $\sum_{j=1}^{\infty} \gamma_j < \infty$ and $\{\phi_j\}_{j=1}^{\infty}$ is the set of trigonometric basis functions, which forms an orthonormal basis of $L^2([0, 1])$. The random variables ξ_j are chosen as $\xi_j \equiv \xi W_j$ where both W_j and ξ are independent $\text{Unif}(-\sqrt{3}, \sqrt{3})$ random variables, so the random function X is non-Gaussian with a bounded range. The eigenvalues are set as $\gamma_j = 2 \sum_{l=j}^{\infty} l^{-5}$, so that the eigengaps $\gamma_j - \gamma_{j+1} = 2j^{-5}$ follow a polynomial decay and give rise to relatively smooth inlier curves.

Eight different types of outlier curves are considered, including one magnitude and seven shape

outliers; [Figure 3](#) displays a realization of the eight types of outliers while ?? in the supplement describes the details of their construction. Note that the shape outliers are set to lie within the range of inliers at any time point, so outlier detection based on single time points will not perform well. Similar outliers have been described in [Dai et al. \(2020\)](#) and the references therein.

4.2 Ranking outliers

We compute the RHD-based normalized rankings of a sample of curves as defined in [Section 2.5](#). Each simulation scenario considers a sample contaminated by a different type of outlier. We consider different sample sizes $n \in \{50, 200, 400\}$, truncation levels $J \in \{2, 4, 6, 8, 10\}$, and regularization parameters corresponding to quantile levels

$u \in \{0.5, \dots, 0.9, 0.91, \dots, 0.99\}$. We only present the results for $n = 400$, $J = 6$, and $u \in \{0.5, 0.7, 0.9, 0.95\}$, and the supplement includes extra results and algorithmic details.

To evaluate the performance of RHD for ranking observations and flagging possible outliers, the normalized rankings of the outlier using different depth notions are compared in [Figure 4](#). The magnitude outlier always has the lowest depth using any depth notion, including the proposed RHD with the smallest regularization parameter ($u = 0.5$) which results in a depth sensitive to only magnitude but not shape outliers. In contrast, the shape outliers, which are harder to detect, have different rankings depending on the depth notions and the tuning parameter λ for RHD. The proposed RHD assigns the smallest depth to most of the shape outliers when λ is large, i.e., $u = 0.9$ or $u = 0.95$, except for the wiggle outlier when $u = 0.9$ and the non-differentiable outlier when either $u = 0.9$ or $u = 0.95$. The MBD, ED, and the first order integrated depth, Nagy₁, do not give the lowest rank to any of the shape outliers, while the second and third order integrated depths, Nagy₂ and Nagy₃, perform quite well in general except for the scenarios with either jump or peak outliers, which have sharp features only in a small time window.

4.3 Outlier detection

We next examine the performance of the proposed outlier detection method based on the RHD. The evaluation metrics are chosen to be the proportion p_c of correctly detected outliers and the

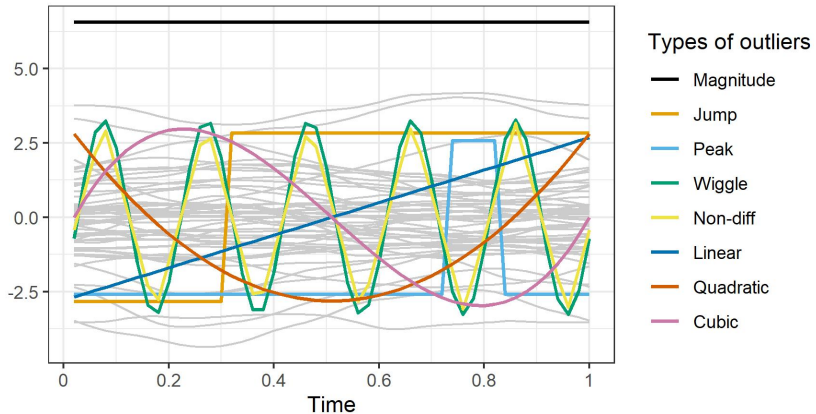


Figure 3: Illustration of the eight types of outliers (black and colored curves) and inliers (gray) considered in the simulation

proportion p_f of falsely detected outliers (Sun and Genton, 2011, Arribas-Gil and Romo, 2014, Dai et al., 2020) averaged over 1000 Monte Carlo experiments. Again, only one type of outlier is added in the sample in each simulation scenario, and for brevity, we display only results for the same case $n = 400$ as presented in Section 4.2; see the Supplementary Materials for the complete results and details. We calculate p_c and p_f for different factors $f \in \{1.5, 2.0, 2.5, 3.0, 3.5\}$ for functional boxplots and for the univariate boxplot in our proposed outlier detection method, but we do not vary the factor $f = 1.5$ in the method by Nagy et al. (2017) since it is set fixed in the R package `ddalpha`.

In Figure 5, we present the results via the receiver operating characteristic (ROC) curve by drawing a scatterplot of p_c versus p_f , where different points on a curve correspond to different factors f , and the color and shape of the dots in the lines indicate the outlier detection method used. First, for the magnitude outlier, our proposed method with smaller regularization parameter ($u = 0.5$) performs very well and is comparable with the other existing methods. Second, for the shape outliers, the functional boxplots with either MBD or ED and our outlier detection method with $u = 0.5$ (the smallest regularization parameter) are powerless in detecting the outliers. In contrast, under larger regularization $u = 0.9$ or $u = 0.95$, our proposed method mostly outperforms all the others. If a larger quantile level such as $u = 0.98$ is chosen, the correct detection rates p_c of RHD-based method for non-differentiable outlier become higher and our method is competitive to the method by Nagy et al. (2017) in this setting; these additional results are given in the supplement. The method proposed by Nagy et al. (2017) performs well in terms of correct detection rates p_c except for the jump and peak outliers, but the false detection rates p_f are relatively high. In summary, our proposed outlier detection method with larger regularization parameters exhibits high p_c and low p_f for all types of shape outliers.

We also show an additional practical scenario where different types of outliers are simultaneously included in the sample. Four types of outliers are selected for this numerical study: magnitude,

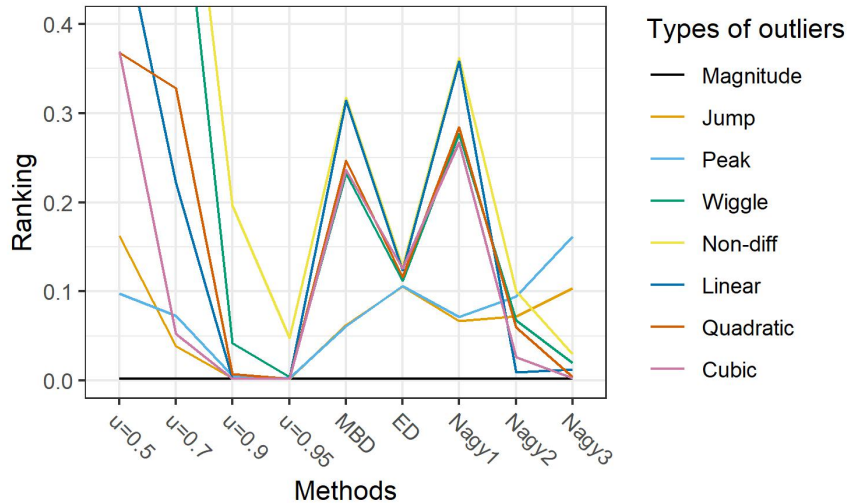


Figure 4: RHD-based normalized rankings of the eight outliers considered from different depth methods when $n = 400$. Lower rank is better since it shows that the outlier can be detected. For the proposed RHD, $J = 6$ and $u \in \{0.5, 0.7, 0.9, 0.95\}$ are considered.

jump, wiggle, and linear outliers. The ROC curve is displayed in [Figure 6](#) for sample size $n = 200$. The truncation level of the proposed RHD is again $J = 6$ and the quantile levels for the

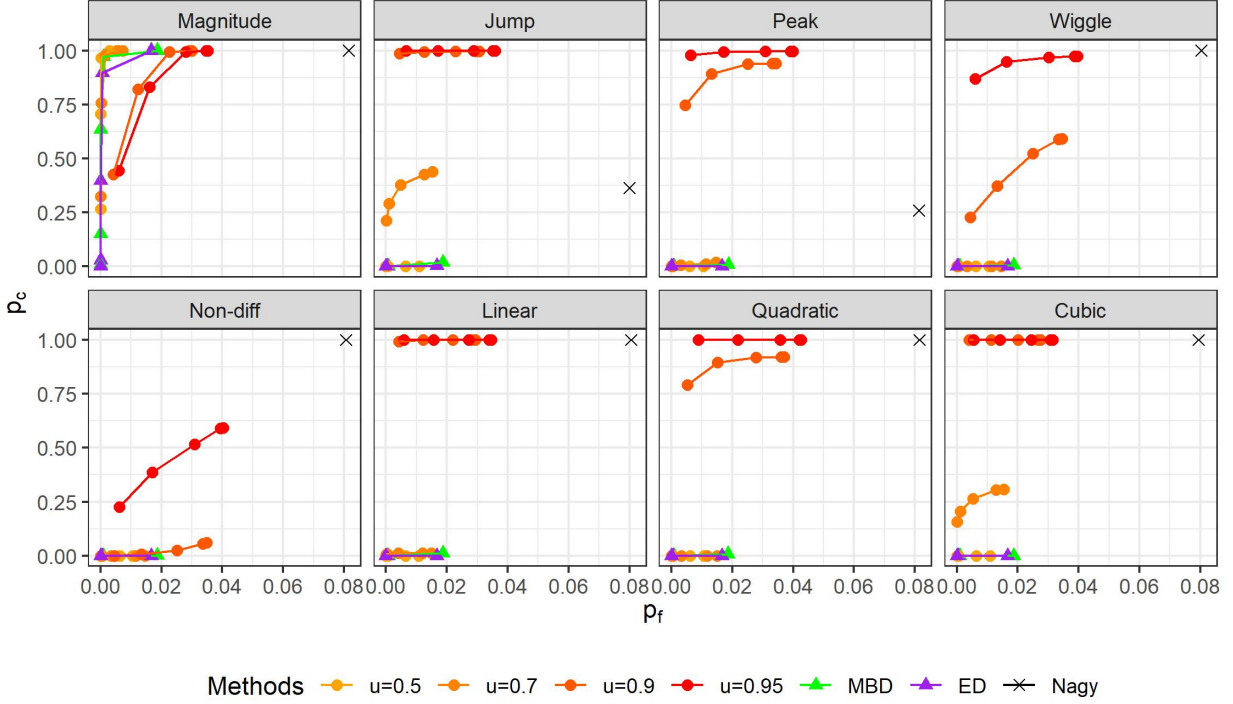


Figure 5: The ROC curves of the proportions of correctly versus falsely detected outliers based on 1000 Monte Carlo iterations. Closer to the upper-left corner indicates better performance. Eight types of outliers are studied, one outlier is included in each dataset and the sample size is $n = 400$. The truncation level is set to be $J = 6$ and four quantile levels $u \in \{0.5, 0.7, 0.9, 0.95\}$ are considered for the proposed RHD.

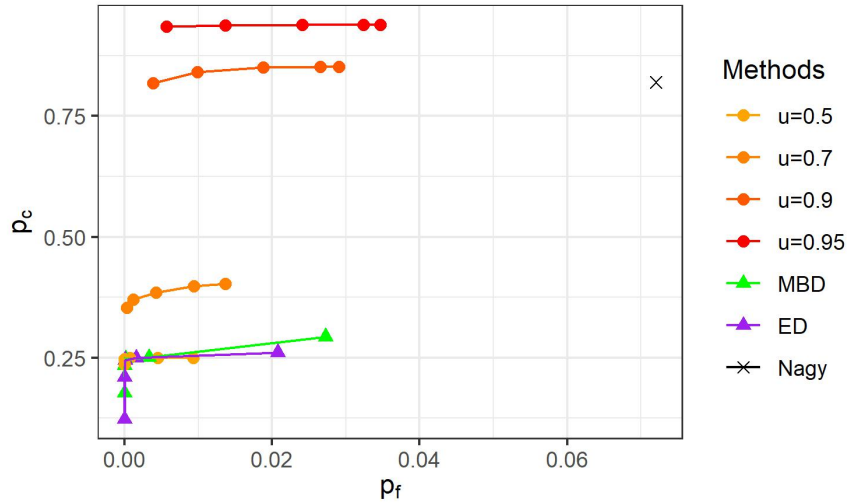


Figure 6: The ROC curves for different outlier detection methods when four shape outliers (magnitude, jump, wiggle, and linear outliers) are simultaneously included in each sample of size $n = 200$. Closer to the upper-left corner indicates better performance. The truncation level is set to be $J = 6$ and four quantile levels $u \in \{0.5, 0.7, 0.9, 0.95\}$ are considered for the proposed RHD.

regularization parameter λ are $u \in \{0.5, 0.7, 0.9, 0.95\}$. In this case, the proposed outlier detection method with large regularization $u = 0.9$ and $u = 0.95$ are superior to the other methods in terms of both p_c and p_f .

5 Data Applications

We apply the RHD-based outlier detection method to real data that exhibit very different characteristics: medfly, world population growth (WPG), and sea surface temperature (SST) datasets. The curves in the medfly example are very dynamic and complex, while the other two datasets consist of smoother and relatively simpler curves that are well-represented by the first few eigenfunctions. For each data example, four regularization parameters $\lambda_1 < \lambda_2 < \lambda_3 < \lambda_4$ based on the quantile levels $u \in \{0.4, 0.6, 0.8, 0.95\}$ and five adjustment factors $\{1.5, 2.0, 2.5, 3.0, 3.5\}$ are considered. In all illustrated figures, outliers are marked in red, while inliers are denoted as dashed grey curves. The deepest curve is marked in blue for reference; if there are multiple deepest curves, we display their average. In this section, we report only the results from the analysis of the medfly dataset while the other results regarding the WPG and SST datasets are deferred to the supplement.

The medfly dataset contains daily observations of number of eggs laid by female Mediterranean fruit flies (medflies, *Ceratitis capitata*) described in [Carey et al. \(1998\)](#). We analyze a subset of $n = 200$ egg-laying trajectories in the first 25 days after hatch (see [Figure 7](#)), randomly selected from a preprocessed dataset containing 789 medflies available in the R package `fdapace`.

Due to the complexity of the medfly trajectories, the functional boxplots constructed with either MBD ([López-Pintado and Romo, 2009](#)) or ED ([Narisetty and Nair, 2016](#)) detect all 200 curves as outliers. Note that MBD and ED are originally defined for smooth functions and might not be appropriate for analyzing very irregular and non-smooth curves. Functional boxplot flags a curve as outlier if it lies outside of the whisker band at any time point, but this does not make sense for this wiggly data because medflies tend to attain very high or low productivity at some random time in their life. In addition, the functional boxplot is hard to read when the curves are often oscillating.

Hence, for this type of data, alternative outlier detection methods are needed to reflect the high variability in the sample. The proposed RHD is defined in the space of square integrable functions, a larger class than the space of smooth functions. Furthermore, our outlier detection method is data-adaptive and measures the outlyingness of each curve depending on the extreme patterns inherent in the samples. Therefore, the proposed outlier detection method based on RHD is adequate to deal with such complex structured curves and in fact performs well as shown next.

[Figure 7](#) displays the outlier detection results from the proposed method with the truncation level $J = 8$ and the adjustment factor $f = 3.5$, which is determined by [??](#). Only the results from $\lambda = \lambda_4 = 0.0507$ are reported here since the method detects no outliers when $\lambda \in \{\lambda_1, \lambda_2, \lambda_3\}$. The proposed method flags three outliers denoted by their IDs in the subsample, 47, 111, and 135. To see their shapes more clearly, we display one outlier in each panel (along with the deepest curve) in the right side of [Figure 7](#). The trajectory for the outlying Medfly 47 is more wiggly than the inliers; Medfly 111 appears to be outlying due to its late start of otherwise high fertility; Medfly 135 has a relatively narrow peak of fertility from day 7 to 12 and then stays lower than most inliers

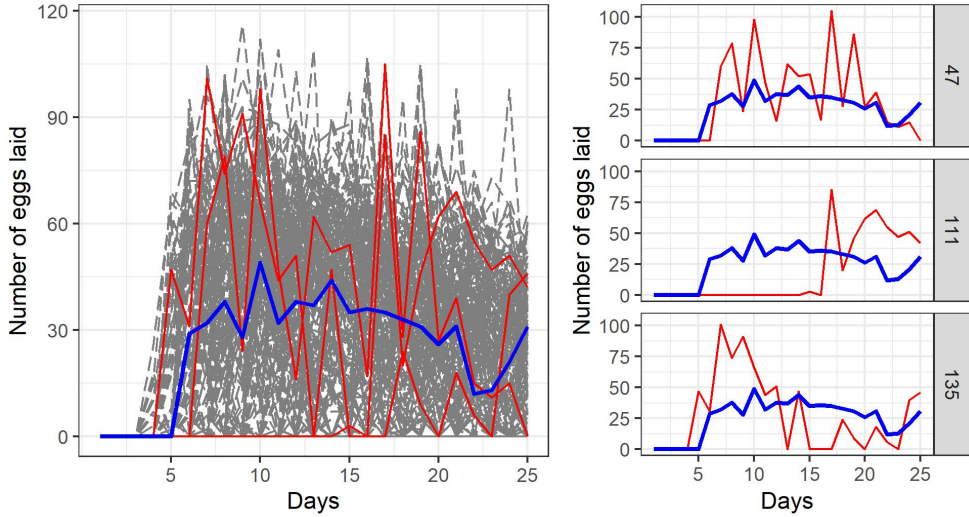


Figure 7: The medfly dataset, showing the outlying curves (red) with IDs 47, 111, and 135 detected by the proposed RHD outlier detection method with the truncation $J = 8$, adjustment factor $f = 3.5$, and regularization $\lambda = \lambda_4 = 0.0507$ (from the quantile level $u = 0.95$). All 200 data curves are exhibited in the left panel with the outliers represented in red and the deepest trajectory in blue. The three flagged outliers are separately displayed in the three sub-panels on the right.

thereafter. These results demonstrate that the RHD and the associated outlier detection method are able to handle non-smooth trajectories without presmoothing and reveal shape outliers with distinct patterns.

Supplementary material

The supplement includes technical details, extra simulation studies, and additional results regarding data applications.

R package

The R-package consists of the following two functions: a function that computes the RHD values and implements the proposed outlier detection procedure as described in Algorithms 1-2; a function that selects the adjustment factor as described in ?? in the supplement.

References

Arribas-Gil, A. and Romo, J. (2014). Shape outlier detection and visualization for functional data: the outliergram, *Biostatistics* **15**(4): 603–619.

Cardot, H., Mas, A. and Sarda, P. (2007). Clt in functional linear regression models, *Probability Theory and Related Fields* **138**(3-4): 325–361.

Carey, J. R., Liedo, P., Müller, H.-G., Wang, J.-L. and Chiou, J.-M. (1998). Relationship of age patterns of fecundity to mortality, longevity, and lifetime reproduction in a large cohort of

mediterranean fruit fly females, *The Journals of Gerontology Series A: Biological Sciences and Medical Sciences* **53**(4): B245–B251.

Chakraborty, A. and Chaudhuri, P. (2014a). On data depth in infinite dimensional spaces, *Annals of the Institute of Statistical Mathematics* **66**(2): 303–324.

Chakraborty, A. and Chaudhuri, P. (2014b). The spatial distribution in infinite dimensional spaces and related quantiles and depths, *The Annals of Statistics* **42**(3): 1203–1231.

Claeskens, G., Hubert, M., Slaets, L. and Vakili, K. (2014). Multivariate functional halfspace depth, *Journal of the American Statistical Association* **109**(505): 411–423.

Cuesta-Albertos, J. A. and Nieto-Reyes, A. (2008). The random Tukey depth, *Computational Statistics & Data Analysis* **52**(11): 4979–4988.

Dai, W. and Genton, M. G. (2018). Multivariate functional data visualization and outlier detection, *Journal of Computational and Graphical Statistics* **27**(4): 923–934.

Dai, W., Mrkvíčka, T., Sun, Y. and Genton, M. G. (2020). Functional outlier detection and taxonomy by sequential transformations, *Computational Statistics & Data Analysis* **149**: 106960.

Donoho, D. L. and Gasko, M. (1992). Breakdown properties of location estimates based on halfspace depth and projected outlyingness, *The Annals of Statistics* **20**: 1803–1827.

Dutta, S., Ghosh, A. K. and Chaudhuri, P. (2011). Some intriguing properties of Tukey’s half-space depth, *Bernoulli* **17**(4): 1420–1434.

Dyckerhoff, R. and Mozharovskyi, P. (2016). Exact computation of the halfspace depth, *Computational Statistics & Data Analysis* **98**: 19–30.

Ghosh, A. K. and Chaudhuri, P. (2005). On data depth and distribution-free discriminant analysis using separating surfaces, *Bernoulli* **11**(1): 1–27.

Gijbels, I. and Nagy, S. (2017). On a general definition of depth for functional data, *Statistical Science* **32**(4): 630–639.

Hall, P., Horowitz, J. L. et al. (2007). Methodology and convergence rates for functional linear regression, *Annals of Statistics* **35**(1): 70–91.

Hsing, T. and Eubank, R. (2015). *Theoretical Foundations of Functional Data Analysis, with an Introduction to Linear Operators*, Vol. 997, John Wiley & Sons.

Hubert, M., Rousseeuw, P. J. and Segaert, P. (2015). Multivariate functional outlier detection, *Statistical Methods & Applications* **24**(2): 177–202.

Hubert, M., Rousseeuw, P. and Segaert, P. (2017). Multivariate and functional classification using depth and distance, *Advances in Data Analysis and Classification* **11**(3): 445–466.

Hyndman, R. J. and Shang, H. L. (2010). Rainbow plots, bagplots, and boxplots for functional data, *Journal of Computational and Graphical Statistics* **19**(1): 29–45.

Kuelbs, J. and Zinn, J. (2013). Concerns with functional depth, *Latin American Journal of Probability and Mathematical Statistics* .

Li, J., Cuesta-Albertos, J. A. and Liu, R. Y. (2012). Dd-classifier: nonparametric classification procedure based on dd-plot, *Journal of the American Statistical Association* **107**(498): 737–753.

Liu, R. Y. (1990). On a notion of data depth based on random simplices, *The Annals of Statistics* pp. 405–414.

Liu, R. Y. (1992). Data depth and multivariate rank tests, *L1-statistical analysis and related methods* pp. 279–294.

Liu, R. Y. and Singh, K. (1993). A quality index based on data depth and multivariate rank tests, *Journal of the American Statistical Association* **88**(421): 252–260.

López-Pintado, S. and Romo, J. (2006). Depth-based classification for functional data, *DIMACS Series in Discrete Mathematics and Theoretical Computer Science* **72**: 103.

López-Pintado, S. and Romo, J. (2009). On the concept of depth for functional data, *Journal of the American Statistical Association* **104**(486): 718–734.

López-Pintado, S., Sun, Y., Lin, J. K. and Genton, M. G. (2014). Simplicial band depth for multivariate functional data, *Advances in Data Analysis and Classification* **8**(3): 321–338.

Nagy, S., Gijbels, I. and Hlubinka, D. (2017). Depth-based recognition of shape outlying functions, *Journal of Computational and Graphical Statistics* **26**(4): 883–893.

Narisetty, N. N. and Nair, V. N. (2016). Extremal depth for functional data and applications, *Journal of the American Statistical Association* **111**(516): 1705–1714.

Nieto-Reyes, A. and Battey, H. (2016). A topologically valid definition of depth for functional data, *Statistical Science* **31**(1): 61–79.

Paindaveine, D. and Van Bever, G. (2013). From depth to local depth: a focus on centrality, *Journal of the American Statistical Association* **108**(503): 1105–1119.

Rousseeuw, P. J., Ruts, I. and Tukey, J. W. (1999). The bagplot: a bivariate boxplot, *The American Statistician* **53**(4): 382–387.

Sguera, C. and López-Pintado, S. (2021). A notion of depth for sparse functional data, *Test* **30**(3): 630–649.

Sun, Y. and Genton, M. G. (2011). Functional boxplots, *Journal of Computational and Graphical Statistics* **20**(2): 316–334.

Sun, Y. and Genton, M. G. (2012). Adjusted functional boxplots for spatio-temporal data visualization and outlier detection, *Environmetrics* **23**(1): 54–64.

Tukey, J. W. (1975). Mathematics and the picturing of data, *Proceedings of the International Congress of Mathematicians, Vancouver, 1975*, Vol. 2, pp. 523–531.

Tukey, J. W. (1977). *Exploratory Data Analysis*, Addison-Wesley: Reading, MA.

Väisälä, J. (2003). A proof of the Mazur-Ulam theorem, *The American mathematical monthly* **110**(7): 633–635.

Wahba, G. (1973). Convergence rates of certain approximate solutions to Fredholm integral equations of the first kind, *Journal of Approximation Theory* **7**(2): 167–185.

Yeh, A. B. and Singh, K. (1997). Balanced confidence regions based on Tukey’s depth and the bootstrap, *Journal of the Royal Statistical Society: Series B* **59**(3): 639–652.

Zuo, Y. and Serfling, R. (2000). General notions of statistical depth function, *The Annals of Statistics* **28**: 461–482.